 CMES, vol.14, no.1, pp.15-29, 2006

Responses of Piezoelectric, Transversely Isotropic, Functionally Graded, and Multilayered Half Spaces to Uniform Circular Surface Loadings

F. Han[1], E. Pan[1], A.K. Roy[2] and Z.Q. Yue[3]

Abstract: In this paper, an analytical solution is presented to study the response of piezoelectric, transversely isotropic, functionally graded, and multilayered half spaces to uniform circular surface loadings (pressure or negative electric charge). The inhomogeneous material is exponentially graded in the vertical direction and can have multiple discrete layers. The propagator matrix method and cylindrical system of vector functions are used to first derive the solution in the transformed domain. In order to find the responses in the physical-domain, which are expressed in one-dimensional infinite integrals of the Bessel function products, we introduced and adopted an adaptive Gauss quadrature. Two piezoelectric functionally graded half-space models are analyzed numerically: One is a functionally graded PZT-4 half space, and the other a multilayered functionally graded half space with two different piezoelectric materials (PZT-4 and PZT-6B). The effect of different exponential factors of the functionally graded material on the field responses is clearly demonstrated. The difference of the responses between the two surface loading cases is also discussed via the numerical examples. The results should be particularly useful in the characterization of material properties using indentation tests, and could indirectly contribute to the design and manufacturing of piezoelectric functionally graded structures.

keyword: Transverse isotropy, Functionally graded material (FGM), Piezoelectric material, Circular surface loading, Multilayered structure, Cylindrical system of vector functions, Propagator matrix method.

1 Introduction

Functionally graded materials (FGMs) were first proposed for the advanced material study in aerospace engineering in 1980s [e.g., Niino, Hirai, and Watanabe (1987)]. Since then FGMs have been applied to various disciplines as diverse as tribology, electronics, and biomechanics [Hirai (1995); Markworth, Ramesh, and Parks (1995); Suresh and Mortensen (1998); Miyamoto, Kaysser, Rabin, Kawasaki, and Ford (1999); Rodel (2003)]. Extending from the purely elastic FGMs, the elastic and electric coupled FGMs were also investigated [Xu, Zhu, and Meng (1999); Almajid and Taya (2001); Almajid, Taya and Hundnut (2001)], and recent preliminary results on fabrication of piezoelectric FGM (PFGM) monomorph, bimorph, and related piezodevices [Almajid and Taya (2001); Almajid, Taya and Hundnut (2001); Chen and Ma (2002); Rodel (2003)] have shown clearly the benefit of using PFGMs.

For the modeling and simulation of the materials and structures properties of FGMs, several numerical and analytical approaches have been proposed. These include the domain-discretization method with special elements [Kim and Paulino (2003); Santare, Thamburaj, and Gazonas (2003); Liew, Yang, and Kitipronchai (2003)], the boundary element method (BEM) [Sutradhar, Paulino, and Gray (2002); Gray, Kaplan, Richardson, and Paulino (2003)], the local boundary integral equation method [Sladek, Sladek, and Atluri (2000)], the meshless local Petrov-Galerkin method [Atluri and Shen (2002)], and the analytical solution to the point-force problem in both 3D and 2D anisotropic elastic FGMs [Martin, Richardson, Gray, and Berger (2002); Chan, Gray, Kaplan, and Paulino (2004)]. While Wang, Tzeng, Pan, and Liao (2003) solved the vertical point-force problem in a transversely isotropic FGM half space, Pan and Han (2005) derived the Green's function of the piezoelectric FGM multilayered half space due to a point source (point force or electric charge density) at any location.

One of the most interesting boundary value problems in multilayered half spaces is the circular surface loading case. This problem has important practical applications in various engineering areas, such as cell biology [Balaban, Schwarz, Riveline, Goichberg, Tzur, Sa-

[1] University of Akron, Akron, OH, U.S.A
[2] AFRL, WPAFB, OH, U.S.A
[3] University of Hong Kong, Hong Kong, China

banay, Mahalu, Safran, Bershadsky, Addadi, and Geiger (2001)], civil engineering [Graig (1997)], foundation engineering [Gerrard and Wardle (1973)], and earth science [Becker and Bevis (2004)]. Furthermore, the solution of the circular loading problem in a layered half space can be also utilized in the indentation test for the material property characterization [e.g., Yu, Sanday, and Rath (1990); Yu (2001); Giannakopoulos and Suresh (1999)]. While numerous analytical/numerical approaches have been proposed for the circular loading solution in inhomogeneous elastic isotropic structures [e.g., Oner (1990); Yue, Yin, and Zhang (1999); Selvadurai (1996); Doherty and Deeks (2003)] and inhomogeneous elastic non-isotropic elastic structures [Hooper (1975); Rowe and Booker (1981); Kumar (1988); Wang, Pan, Tzeng, Han, and Liao (2005)], to the best of the authors' knowledge, however, no solution exists for the corresponding circular loading in a piezoelectric transversely isotropic multilayered half-space with FGMs.

This paper is therefore to derive the solution for the multilayered and transversely isotropic PFGM half spaces subjected to the circular loading applied on the surface. First, by virtue of the cylindrical systems of vector functions and the propagator matrix method [Gilbert and Backus (1966); Pan (1989a,b); Pan (1997); Pan and Han, 2004], we obtain the layer solution and propagator matrices in the transformed domain. Then, we utilize the propagator matrix method to propagate the solution from one layer to the other directly and efficiently. Finally, we calculate the physical-domain solution by introducing and modifying an adaptive Gauss quadrature [Chave (1983); Lucas (1995)]. This paper is organized as follows: In Section 2, we state the problem with the corresponding governing equations. In Section 3, the general layer solution and propagator matrices are derived in the transformed domain. The boundary conditions for the surface circular loading case are presented in Section 4, along with the expansion coefficients in the transformed domain. While Section 5 presents the solution in the transformed domain, Section 6 discusses the integration issue on obtaining the physical-domain solution. Numerical examples are presented in Section 7 and conclusions are drawn in Section 8.

2 Problem statement

Let us consider a structure made up of N parallel, transversely isotropic PFGM layers lying over a transversely isotropic PFGM half space. The layers are numbered serially with the layer at the top being layer 1 and the last layer N, which is just above the half space (Fig. 1). We assume that in each layer the PFGM has a locally varied microstructure described by an exponential variation in the vertical direction, i.e., $e^{\eta\zeta}$, with ζ being the local vertical variable and η the FGM exponential factor (Fig. 1). While $\eta = 0$ reduces to the homogeneous material case, different variations in the vertical direction can be approximated using different exponential factor η. We place the global cylindrical coordinates on the surface with the z-axis pointing into the layered half space. The k-th layer is bounded by the interfaces $z = z_{k-1}, z_k$. As such, z_{k-1} is the vertical coordinate of the upper interface of the k-th layer, and z_k that of the lower interface. It is obvious that z_0= 0 and $z_p = H$, where H is the depth of the last layer interface. In each layer, we also place a local vertical coordinate ζ (Fig. 1 for the k-th layer), which is actually a measure of the distance from the upper interface of the layer.Obviously, for the k-th layer with a thickness h_k, the relation between the local and global coordinates is: $\zeta = z - z_{k-1} (0 \le \zeta \le h_k)$. We further assume that the only load considered in this paper is the surface load applied within a circle and that all the interfaces are perfect (i.e., with continuous traction and normal electric displacement component).

For transversely isotropic PFGMs, we have in each layer, the following governing equations:

1). Equilibrium equations (without body force or electric charge density)

$$\sigma_{ij,j} = 0; \tag{1a}$$

$$D_{i,i} = 0 \tag{1b}$$

where σ_{ij} and D_i are the stress and electric displacement, respectively.

2). Constitutive relations

$$\begin{aligned}
\sigma_{rr} &= C_{11}\gamma_{rr} + C_{12}\gamma_{\theta\theta} + C_{13}\gamma_{zz} - e_{31}E_z \\
\sigma_{\theta\theta} &= C_{12}\gamma_{rr} + C_{11}\gamma_{\theta\theta} + C_{13}\gamma_{zz} - e_{31}E_z \\
\sigma_{zz} &= C_{13}\gamma_{rr} + C_{13}\gamma_{\theta\theta} + C_{33}\gamma_{zz} - e_{33}E_z \\
\sigma_{\theta z} &= 2C_{44}\gamma_{\theta z} - e_{15}E_\theta \\
\sigma_{rz} &= 2C_{44}\gamma_{rz} - e_{15}E_r \\
\sigma_{r\theta} &= 2C_{66}\gamma_{r\theta}
\end{aligned} \tag{2a}$$

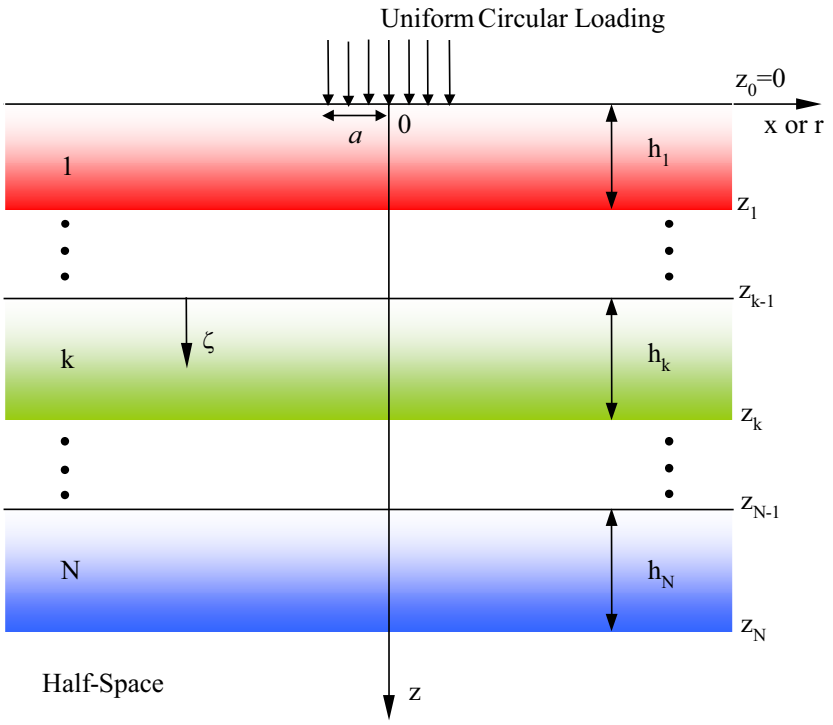

Figure 1 : Geometry of a PFGM multilayered half space subject to a uniform surface load within the circle of $r = a$. Both vertical global (z) and local (ζ) coordinates are attached to the layered half space.

$$D_r = 2e_{15}\gamma_{rz} + \varepsilon_{11}E_r$$
$$D_\theta = 2e_{15}\gamma_{\theta z} + \varepsilon_{11}E_\theta \tag{2b}$$
$$D_z = e_{31}(\gamma_{rr} + \gamma_{\theta\theta}) + e_{33}\gamma_{zz} + \varepsilon_{33}E_z$$

where γ_{ij} is the elastic strain and E_i the electric field; C_{ij}, e_{ij} and ε_{ij} are the elastic moduli, piezoelectric coefficients, and dielectric coefficients, respectively. We remark that the solutions derived in this paper include those for the corresponding elastic FGM media as a special case (by setting the piezoelectric coefficients e_{ij} to zero).

3). Elastic displacement-strain and electric potential-electric field relations

$$\gamma_{ij} = 0.5(u_{i,j} + u_{j,i}); \tag{3a}$$
$$E_i = -\phi_{,i} \tag{3b}$$

where u_i and ϕ are the elastic displacement and electric potential, respectively.

For any PFGM layer with an exponential variation in the z- (or ζ-) direction, the material coefficients in (2a) and (2b) can be described by

$$C_{ik}(\zeta) = C^0_{ik}e^{\eta\zeta};\ \ \varepsilon_{ik}(\zeta) = \varepsilon^0_{ik}e^{\eta\zeta};\ e_{ik}(\zeta) = e^0_{ik}e^{\eta\zeta} \tag{4}$$

where η again is the exponential factor characterizing the degree of material gradient in the z- (or ζ-) direction, and the superscript 0 is attached to indicate the z-independent factor in the material coefficient. Again, $\eta = 0$ corresponds to the homogeneous material case.

For transversely isotropic PFGMs, the material coefficients in the constitutive relations (2a) and (2b) can be expressed as

$$[C] = \begin{bmatrix} C^0_{11} & C^0_{12} & C^0_{13} & 0 & 0 & 0 \\ & C^0_{22} & C^0_{23} & 0 & 0 & 0 \\ & & C^0_{33} & 0 & 0 & 0 \\ & & & C^0_{44} & 0 & 0 \\ & Sym & & & C^0_{44} & 0 \\ & & & & & (C^0_{11} - C^0_{12})/2 \end{bmatrix} e^{\eta\zeta} \tag{5a}$$

$$[e] = \begin{bmatrix} 0 & 0 & 0 & 0 & e^0_{15} & 0 \\ 0 & 0 & 0 & e^0_{15} & 0 & 0 \\ e^0_{31} & e^0_{31} & e^0_{33} & 0 & 0 & 0 \end{bmatrix} e^{\eta\zeta} \tag{5b}$$

$$[\varepsilon] = \begin{bmatrix} \varepsilon^0_{11} & 0 & 0 \\ 0 & \varepsilon^0_{11} & 0 \\ 0 & 0 & \varepsilon^0_{33} \end{bmatrix} e^{\eta\zeta} \tag{5c}$$

Taking the advantage of the axis-symmetry condition, the solution can be conveniently expressed in terms of the cylindrical system of vector functions (Pan, 1989a,b; Pan and Han, 2005):

$$\mathbf{L}(r,\theta;\lambda,m) = \mathbf{e}_z S(r,\theta;\lambda,m)$$

$$\mathbf{M}(r,\theta;\lambda,m) = (\mathbf{e}_r \frac{\partial}{\partial r} + \mathbf{e}_\theta \frac{\partial}{r\partial\theta}) S(r,\theta;\lambda,m) \tag{6}$$

$$\mathbf{N}(r,\theta;\lambda,m) = (\mathbf{e}_r \frac{\partial}{r\partial\theta} - \mathbf{e}_\theta \frac{\partial}{\partial r}) S(r,\theta;\lambda,m)$$

with

$$S(r,\theta;\lambda,m) = \frac{1}{\sqrt{2\pi}} J_m(\lambda r) e^{im\theta} \tag{7}$$

where $\boldsymbol{e}_r$, $\boldsymbol{e}_\theta$, and $\boldsymbol{e}_z$ are the unit vectors along the $r-$, $\theta-$, and $z-$ (or $\zeta-$) axes, respectively; $J_m(\lambda r)$ is the Bessel function of order m with m = 0 corresponding to the axial symmetric deformation. This cylindrical system of vector functions possesses certain special and advanced features as compared to the direct Hankel transform [Pan and Han (2005)].

3 General solution and propagator matrix of each layer

In order to derive the general solution for each layer, say layer k, we first express the elastic displacement, electric potential, traction, and electric displacements in terms of the cylindrical system of vector functions (6) (omitting the dependence of the integration on the integral variables λ and m):

$$\boldsymbol{u}(r,\theta,z) = \sum_m \int_0^{+\infty} [U_L(z)\boldsymbol{L}(r,\theta) + U_M(z)\boldsymbol{M}(r,\theta) + U_N(z)\boldsymbol{N}(r,\theta)]\lambda d\lambda \tag{8a}$$

$$\phi(r,\theta,z) = \sum_m \int_0^{+\infty} \Phi(z) S(r,\theta)\lambda d\lambda \tag{8b}$$

$$\begin{aligned}\boldsymbol{t}(r,\theta,z) &\equiv \sigma_{rz}\boldsymbol{e}_r + \sigma_{\theta z}\boldsymbol{e}_\theta + \sigma_{zz}\boldsymbol{e}_z \\ &= \sum_m \int_0^{+\infty} [T_L(z)\boldsymbol{L}(r,\theta) \\ &\quad + T_M(z)\boldsymbol{M}(r,\theta) + T_N(z)\boldsymbol{N}(r,\theta)]\lambda d\lambda\end{aligned} \tag{8c}$$

$$\boldsymbol{D}(r,\theta,z) = \sum_m \int_0^{+\infty} [D_L(z)\boldsymbol{L}(r,\theta) + D_M(z)\boldsymbol{M}(r,\theta) + D_N(z)\boldsymbol{N}(r,\theta)]\lambda d\lambda \tag{8d}$$

Taking the derivatives of the elastic displacement (8a) and electric potential (8b), substituting the results into the constitutive relations (2a,b) and the equilibrium equations (1a,b), the following sets of first-order differential equations can be derived [Pan and Han (2005)]:

$$\frac{dT_L}{dz} - \lambda^2 T_M = 0 \tag{9a}$$

$$(-\lambda^2 C_{11}^0 U_M + C_{13}^0 \frac{dU_L}{dz} + e_{31}^0 \frac{d\Phi}{dz}) e^{\eta\zeta} + \frac{dT_M}{dz} = 0 \tag{9b}$$

$$\frac{dT_N}{dz} - \lambda^2 C_{66}^0 U_N e^{\eta\zeta} = 0 \tag{9c}$$

$$\frac{dD_L}{dz} - \lambda^2 e_{15}^0 (\frac{dU_M}{dz} + U_L) e^{\eta\zeta} + \lambda^2 \varepsilon_{11}^0 \Phi e^{\eta\zeta} = 0 \tag{9d}$$

In Eq. 9, ζ again is the local vertical coordinate within the PFGM layer indicating the exponential variation with depth. It is clear that for axial symmetric circular surface pressure or electric charge, we only need to consider the LM-type problem and its corresponding solutions. We present the key steps below.

First, Eq. 9 can be recast into a compact form of equations as

$$[U_L, U_M, T_L, T_M, \Phi, D_L]_{,z}^t = [A][U_L, U_M, T_L, T_M, \Phi, D_L]^t \tag{10}$$

where the nonzero elements of the 6×6 matrix $[\boldsymbol{A}]$ can be found in Pan and Han (2005). It is remarked that all the diagonal elements of $[\boldsymbol{A}]$ are zero, a feature that is very useful in the eigenvalues/eigenvectors analysis.

Secondly, we temporarily introduce the following vector

$$[\boldsymbol{E}^*] = [U_L, \lambda U_M, T_L e^{-\eta\zeta}/\lambda, T_M e^{-\eta\zeta}, \Phi, D_L e^{-\eta\zeta}/\lambda]^t \tag{11}$$

so that Eq. 10 can be rewritten as

$$[\boldsymbol{E}^*]_{,z} = \lambda[W][\boldsymbol{E}^*] \tag{12}$$

Again, the nonzero elements of the 6×6 matrix $[\boldsymbol{W}]$ in Eq. 12 can be found in Pan and Han (2005). It is noticed that matrix $[\boldsymbol{W}]$ is independent of the vertical coordinate z or ζ, and it depends only upon the parameters η and λ as well as the constant elastic coefficients.

Thirdly, in order to find the homogeneous solution of Eq. 12, we assume that

$$[\boldsymbol{E}^*(\zeta)] = [\boldsymbol{b}] e^{\lambda\nu\zeta} \tag{13}$$

Substituting Eq. 13 into Eq. 12 and noticing that all the diagonal elements of $[\boldsymbol{W}]$ are zero gives us the following eigenequation system of 6×6

$$\{[W]-v[I]\}[\boldsymbol{b}]=0 \tag{14}$$

where $[\boldsymbol{I}]$ is the 6×6 identity matrix.

We remark that the eigenvalues and their corresponding eigenvectors of Eq. 14 depend on the integral variable λ and the PFGM exponential factor η. Therefore, these eigenequations need to be solved for different η and for each integration point λ.

Fourthly, assuming that the 6 eigenvalues v_i are distinct, the general solution of Eq. 12 is found to be

$$[\boldsymbol{E}^*(z)]=[Z(z)][\boldsymbol{K}] \tag{15}$$

where $[\boldsymbol{K}]$ is a 6×1 coefficient matrix with its elements to be determined by the interface and/or boundary conditions, and

$$[Z(z)]=[B]\left\langle e^{\lambda \mathrm{V}*\zeta}\right\rangle \tag{16}$$

with

$$\left\langle e^{\lambda \mathrm{V}*\zeta}\right\rangle = diag[e^{\lambda v_1\zeta}, e^{\lambda v_2\zeta}, e^{\lambda v_3\zeta}, e^{\lambda v_4\zeta}, e^{\lambda v_5\zeta}, e^{\lambda v_6\zeta}] \tag{17}$$

$$[B]=[\boldsymbol{b}_1,\boldsymbol{b}_2,\boldsymbol{b}_3,\boldsymbol{b}_4,\boldsymbol{b}_5,\boldsymbol{b}_6] \tag{18}$$

It is noted that the real parts of the first three eigenvalues are positive and those of the remaining three are negative.

Fifthly, in order to use the propagating relation for the PFGM multilayered structure, we introduce the following new set of coefficients:

$$[\boldsymbol{E}]=[U_L,\lambda U_M,T_L/\lambda,T_M,\Phi,D_L/\lambda]^t \tag{19}$$

which is related to $[\boldsymbol{E}^*]$ as

$$[\boldsymbol{E}]=\langle P\rangle[\boldsymbol{E}^*] \tag{20}$$

where $\langle \mathrm{P}\rangle$ is a 6×6 diagonal matrix defined as

$$\langle P\rangle = diag[1,1,e^{\eta\zeta},e^{\eta\zeta},1,e^{\eta\zeta}] \tag{21}$$

Finally, the propagating relation in terms of the coefficient vector $[\boldsymbol{E}]$ of k-th layer, which connects the values at the global coordinate z_{k-1} ($\zeta=0$) to those at z_k($\zeta=h_k$), is found to be

$$[\boldsymbol{E}(z_{k-1})]=[a][\boldsymbol{E}(z_k)] \tag{22}$$

where

$$[a]=[B]\left\langle e^{-\lambda \mathrm{V}*h_k}\right\rangle [B]^{-1}\langle \mathrm{Q}\rangle \tag{23}$$

is the propagator matrix for the LM-type deformation, and

$$\left\langle e^{-\lambda \mathrm{V}*h_k}\right\rangle = diag[e^{-\lambda v_1h_k},e^{-\lambda v_2h_k},e^{-\lambda v_3h_k},e^{-\lambda v_4h_k}, e^{-\lambda v_5h_k},e^{-\lambda v_6h_k}] \tag{24}$$

$$\langle Q\rangle = diag[1,1,e^{-\eta_kh_k},e^{-\eta_kh_k},1,e^{-\eta_kh_k}] \tag{25}$$

We point out that in solving the eigenequation (14), we have assumed that all the eigenvalues are distinct. Should repeated eigenvalues occur, a slight perturbation on the material properties can be used to make all the eigenvalues distinct with neglected errors so that the solution developed in this paper can still be used directly.

4 Circular surface loading in the transformed domain

We assume that the top surface of the multilayered half space is subject to a uniform load within the circle of radius a(Fig. 1). Depending on whether a pressure p or a negative electric charge $-Q$ is applied, we have the following two loading cases.

4.1 Loading case 1

A uniform pressure is applied, along with the zero normal component of the electric displacement D_z=0. Obviously, the traction boundary condition on the surface (z=0) can be expressed as:

$$\sigma_{zz}=\begin{cases} p & r<a \\ 0 & r>a \end{cases} \tag{26}$$

$$\sigma_{rz}=\sigma_{\theta z}=0\ 0\le r\le\infty$$

Substituting Eq. 26 to the vector function expansion for the traction Eq. 8c and taking the inverse Hankel transformation, we obtain the expansion coefficients at the surface z=0 due to the uniform pressure p, along with the zero normal electric displacement condition

$$T_L(\lambda,0)=-2\pi paJ_1(\lambda a) \tag{27}$$

$$T_M(\lambda,0)=D_L(\lambda,0)=0$$

4.2 Loading case 2

A normal electric displacement is applied, along with the zero traction condition σ_{rz}=$\sigma_{\theta z}$=σ_{zz}=0. For this case, the normal electric displacement component on the surface (z=0) can be expressed as:

$$D_z = \begin{cases} -Q & r < a \\ 0 & r > a \end{cases} \tag{28}$$

Similarly, the surface expansion coefficients due to this uniform electric charge, along with the traction-free boundary condition, are:

$$D_L(\lambda,0) = 2\pi Q a J_1(\lambda a) \tag{29}$$

$$T_L(\lambda,0) = T_M(\lambda,0) = 0$$

With these given boundary conditions on the surface z=0, we can then find the solution of the problem in the transformed domain (i.e., in terms of the expansion coefficients).

5 Transformed-domain solutions

For the whole PFGM multilayered structure, propagating the solutions from the half space $z = H$ to the surface z=0, we obtain

$$[\boldsymbol{E}(0)] = [G][\boldsymbol{K}_N] \tag{30}$$

where

$$[G] = [a_1][a_2] - - - [a_N][Z_N(H)] \tag{31}$$

and the undetermined coefficients have the structure as

$$[\boldsymbol{K}_N] = [0,0,0,*,*,*]^t \tag{32}$$

where the symbol '*' represents the coefficient to be determined. The structure of Eq. 32 is chosen to satisfy the requirement that the solution vanishes when z approaches $+\infty$.

Using the boundary condition Eq. 27 or Eq. 29, the unknown coefficients in $[\boldsymbol{K}_N]$ can be determined, since in either case, we have three conditions to determine the three unknowns in $[\boldsymbol{K}_N]$. With the solved coefficients in $[\boldsymbol{K}_N]$, the expansion coefficients at any depth z ($z_{k-1} \le z \le z_k$) can be obtained exactly as:

$$[\boldsymbol{E}(z)] = [a_{k2}(z - z_{k-1})][a_{k+1}] \\ - - - [a_N][Z_N(H)][\boldsymbol{K}_N] \tag{33}$$

As discussed in Pan (1997) and Yue and Yin (1998), overflow may occur from multiplication of matrices in Eq. 31 and Eq. 33. This can be overcome by factoring out the exponentially growing factor in the elements of the propagator matrix. Since in the modified propagator matrices, no element is exponentially growing, there will be no overflow problem for a multilayered half space having any number of layers with any thickness for each layer.

6 Physical-domain solutions

The transformed-domain solutions presented above can be integrated numerically to find the corresponding physical-domain solutions. In terms of the cylindrical system of vector functions, the individual component of the field quantities will be in the cylindrical coordinates.

Since the given boundary load T_L or D_L in the transformed domain involves the Bessel function of first order (Eq. 27 and Eq. 29), all the integrands under the 1D infinite integral will be the product of Bessel functions. It is further noted that the product of Bessel functions are oscillatory and goes to zero slowly when its variable approaches infinity. Thus, the common numerical integral methods, such as the trapezoidal or Simpson rule, are not suitable for such integrations. However, numerical integration of this type of functions via the adaptive Gauss quadrature [Chave (1983); Lucas (1995)] has been found to be very accurate and efficient. We therefore have adopted and modified this algorithm to the evaluation of the field responses in the PFGM multilayered half space.

Let us express the infinite integral for each field response as a summation of partial integration terms:

$$\int_0^{+\infty} f(\lambda,z) J_m(\lambda r) J_1(\lambda a) d\lambda \\ = \sum_{n=1}^{N} \int_{\lambda_n}^{\lambda_{n+1}} f(\lambda,z) J_m(\lambda r) J_1(\lambda a) d\lambda \tag{34}$$

In each subinterval, a starting 3-point Gauss rule is applied to approximate the integral. A combined relative-absolute error criterion is used to check the results. If the error criterion is not satisfied, new Gauss points are added optimally so that only the new integrand values need to be calculated. This procedure continues until the

Table 1 : Different loading cases and different material models

Loading Cases (circular radius a =1m)	Case 1	Uniform pressure p (=1N/m^2)
	Case 2	Uniform negative electric charge $-Q$ (= $-$1C/m)
Material Models	Model 1	PFGM half space made of PZT-4
	Model 2	Multilayered half space with stacking sequence FGM PZT-4/PZT-6B/PZT-4

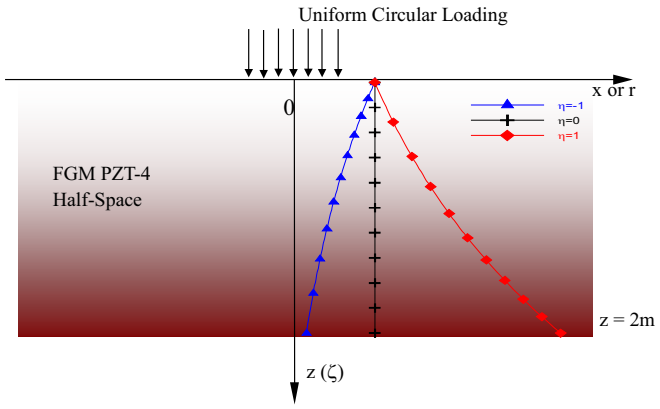

Figure 2 : Geometry of the PFGM PZT-4 half space for material Model 1. The variation of the proportional factor $e^{\eta z}$ in the PFGM half space is shown for η = -1, 0, 1.

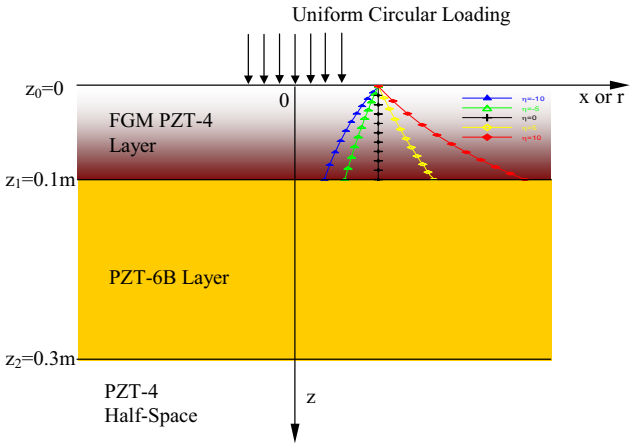

Figure 3 : Geometry of the PFGM multilayered half space for material Model 2, with stacking sequence of FGM PZT-4/PZT-6B/PZT-4. The variation of the proportional factor $e^{\eta z}$ in the FGM PZT-4 layer is shown for η = -10, -5, 0, 5, 10.

selected error criterion is satisfied [Lucas (1995)]. In the numerical analysis presented below, we have set the relative and absolute errors, respectively, at 10^{-4} and 10^{-5}. Further discussion on this type of oscillatory integration can also be found in Pan, Bevis, Han, Zhou, and Zhu (2006).

7 Numerical examples

Before applying our PFGM multilayered solution to the numerical examples presented below, we have first checked various reduced cases. For instance, we reduced our solution to the corresponding purely elastic FGM half space (i.e., the piezoelectric coefficient e_{ij}=0) and piezoelectric layered homogeneous (i.e., the exponential factor η = 0) solutions, and we found that the results from the present PFGM multilayered half-space solutions due to a uniform circular pressure are the same as those from previous solutions [Wang, Fang, and Chen (2002); Wang, Pan, Tzeng, Han, and Liao (2005)].

In our numerical studies, the PFGM layered half space is made of two transversely isotropic piezoelectric materials: One is the poled lead-zirconate-titanate (PZT-4) ceramic and the other is PZT-6B, with their material properties given in the Appendix A. Two different PFGM layered half-space models are studied in this paper (Tab. 1): In material Model 1 (Fig. 2), we have a single PFGM half space made of FGM PZT-4, and the response contour is in the vertical plane (y = 0) for x and z varying from 0 to 2m. In material Model 2 (Fig. 3), we have a multilayered half space with stacking sequence FGM PZT-4/PZT-6B/PZT-4. The first layer is functionally graded PZT-4 with thickness 0.1m, the second layer is homogeneous PZT-6B with thickness 0.2m, and the last layer is a homogeneous PZT-4 half space. The observation point is

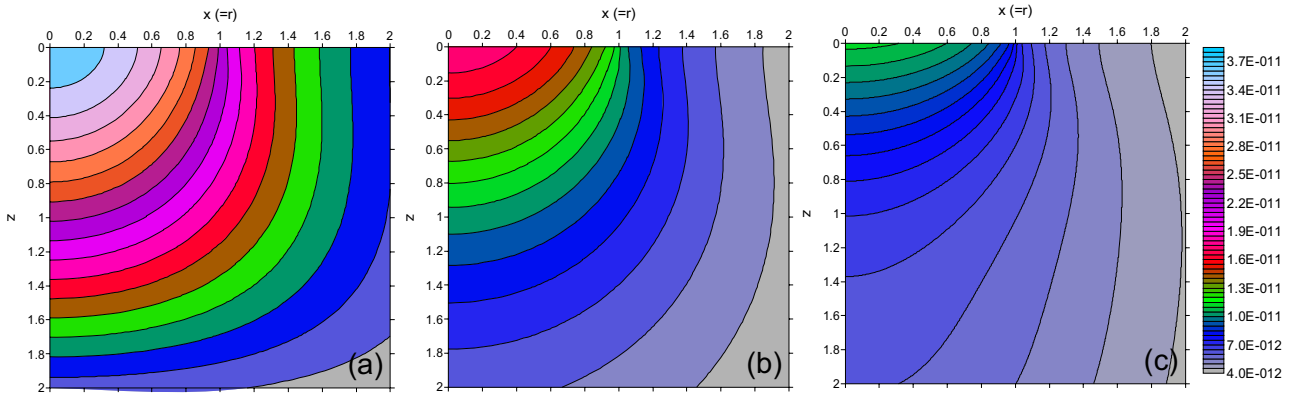

Figure 4 : Contours of the vertical elastic displacement u_z in material Model 1 due to the uniform surface pressure within the circle of a=1m and magnitude of 1N/m^2 (Case 1). Figures (a), (b), (c) show, respectively, the results for exponential factor η = -1, 0, and 1.

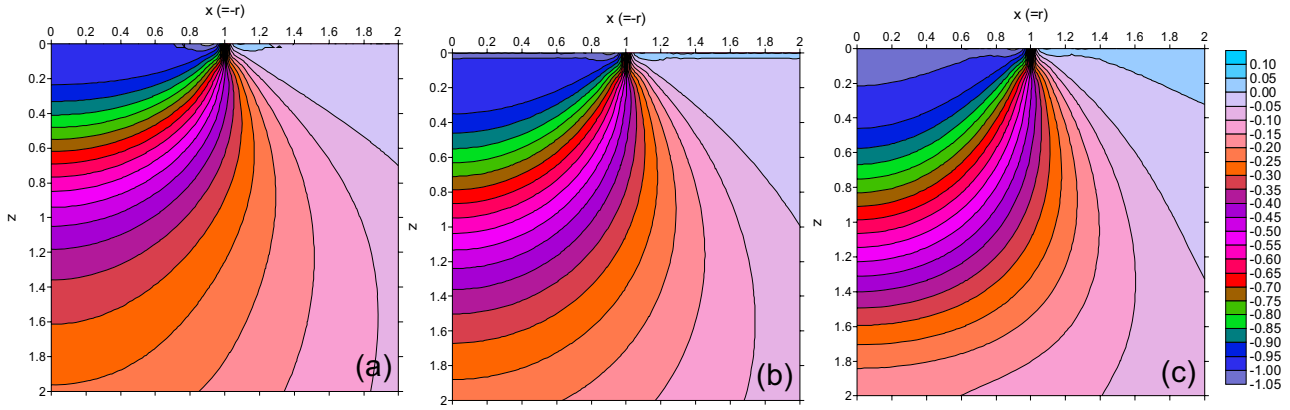

Figure 5 : Contours of the vertical stress σ_{zz} in material Model 1 due to the uniform surface pressure within the circle of a=1m and magnitude of 1N/m^2 (Case 1). Figures (a), (b), (c) show, respectively, the results for exponential factor η = -1, 0, and 1.

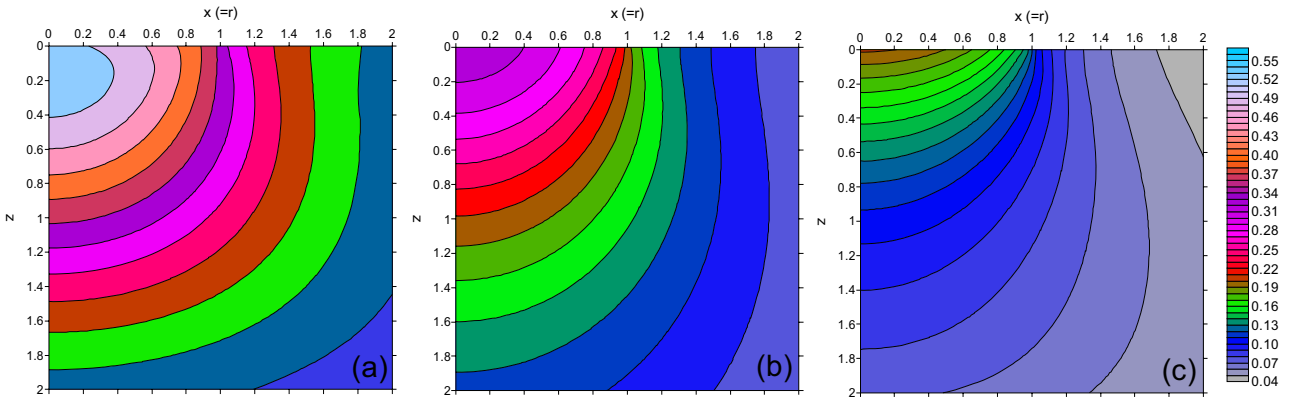

Figure 6 : Contours of the electric potential ϕ in material Model 1 due to the uniform surface pressure within the circle of a=1m and magnitude of 1N/m^2 (Case 1). Figures (a), (b), (c) show, respectively, the results for exponential factor η = -1, 0, and 1.

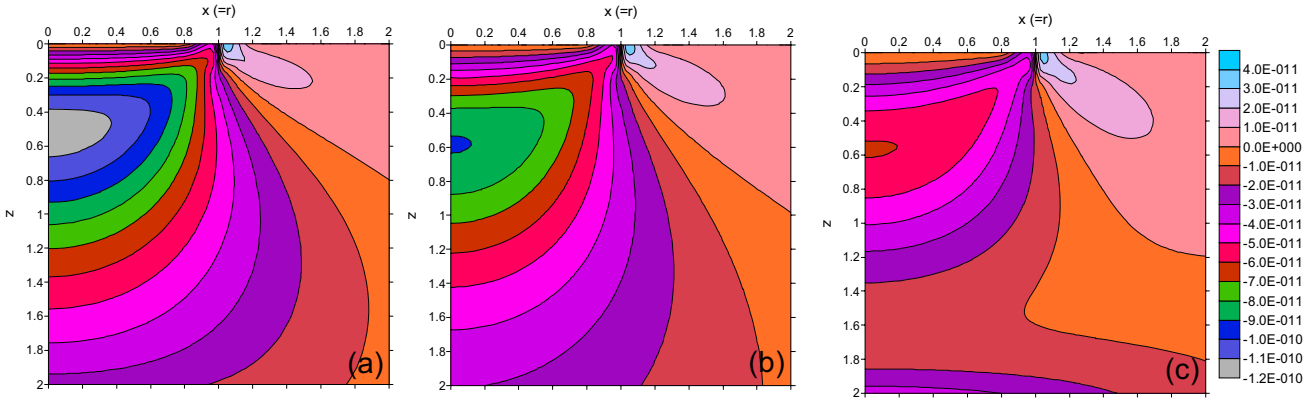

Figure 7 : Contours of the vertical electric displacement D_z in material Model 1 due to the uniform surface pressure within the circle of a=1m and magnitude of 1N/m^2 (Case 1). Figures (a), (b), (c) show, respectively, the results for exponential factor η = -1, 0, and 1.

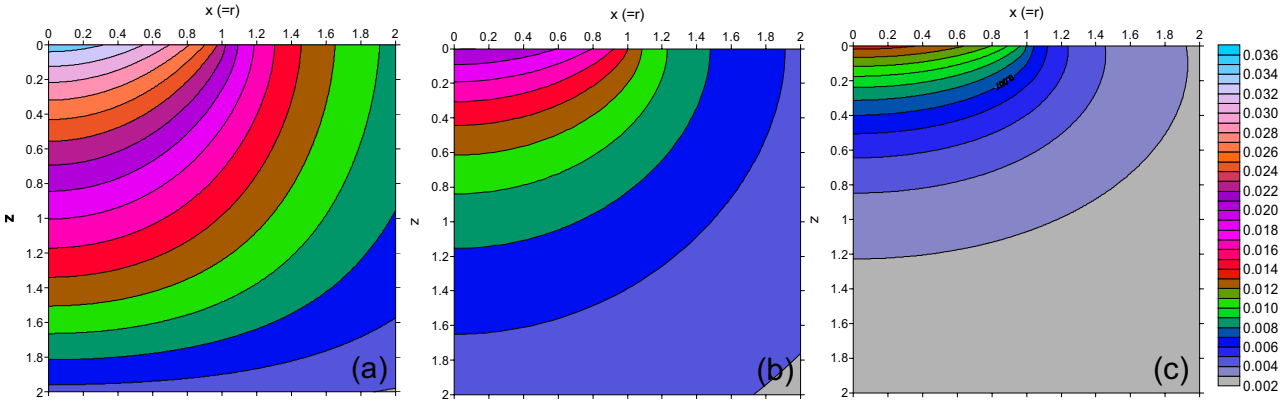

Figure 8 : Contours of the vertical elastic displacement u_z in material Model 1 due to the uniform negative charge within the circle of a=1m and magnitude of 1C/m (Case 2). Figures (a), (b), (c) show, respectively, the results for exponential factor η = -1, 0, and 1.

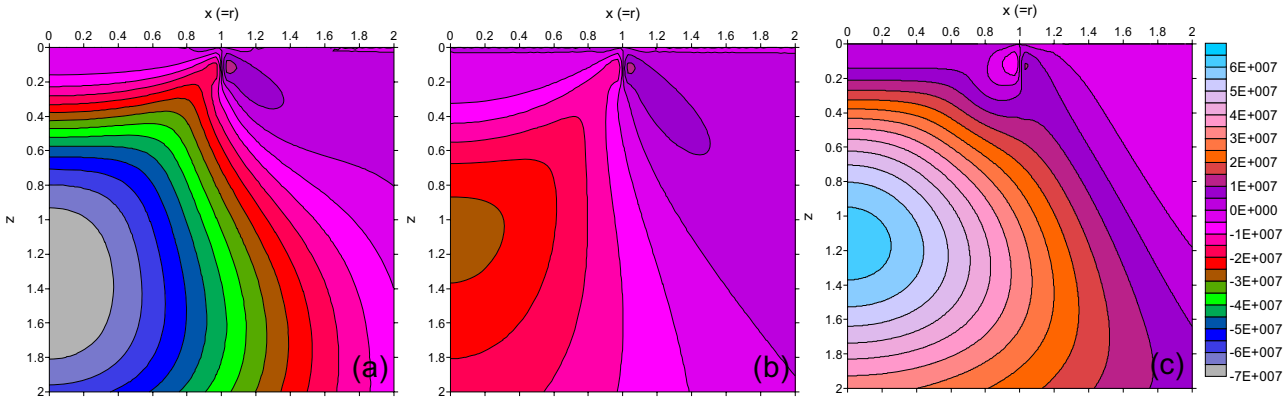

Figure 9 : Contours of the vertical stress σ_{zz} in material Model 1 due to the uniform negative charge within the circle of a=1m and magnitude of 1C/m (Case 2). Figures (a), (b), (c) show, respectively, the results for exponential factor η = -1, 0, and 1.

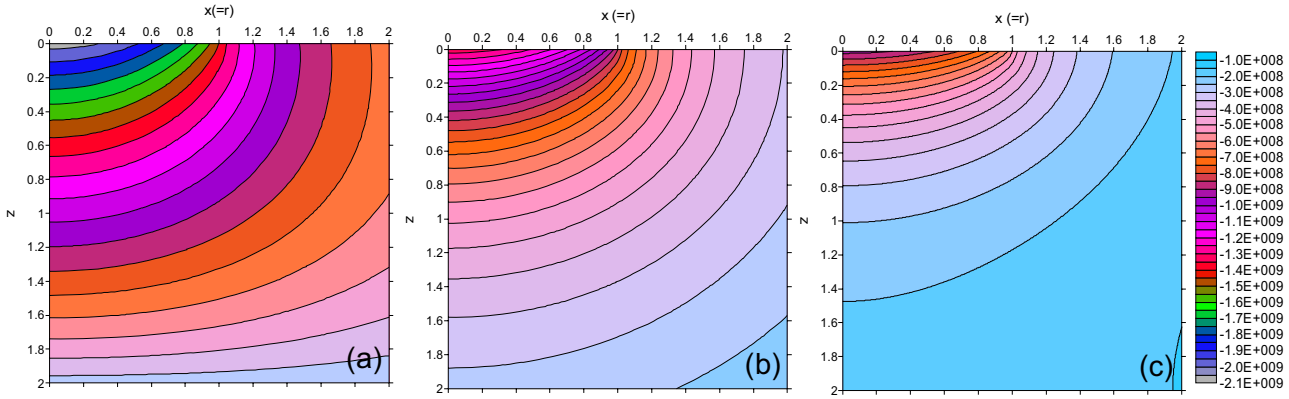

Figure 10 : Contours of the electric potential ϕ in material Model 1 due to the uniform negative charge within the circle of a=1m and magnitude of 1C/m (Case 2). Figures (a), (b), (c) show, respectively, the results for exponential factor η = -1, 0, and 1.

along the z-axis from the surface (z=0) to the half space (z=0.5m). For the two different material Models, two different loading Cases on the surface within radius a (=1m) are studied (Tab. 1): under uniform pressure p (=1N/m^2) for Case 1 and under uniform negative electric charge $-Q$ (= $-$1C/m) for Case 2. We remark that all the results presented below are dimensionless. In order to find the corresponding dimensional value from the dimensionless result, one just needs to multiply the suitable convert constants [Pan (2002); Pan and Han (2005)].

7.1 Response of the PFGM half space to loading Cases 1 and 2

This PFGM half space corresponds to the material Model 1, which is made of FGM PZT-4 (Fig. 2). Fig. 4 to Fig. 7 show, respectively, contours of the vertical elastic displacement u_z, vertical normal stress σ_{zz},electric potential ϕ, and vertical electric displacement D_z in the plane y=0 due to a uniform circular pressure of magnitude 1N/m^2 applied on the surface (Case 1 loading). Similarly, Fig. 8 to Fig. 11 show the corresponding contours due to a uniform circular negative charge of magnitude –1C/m applied on the surface (Case 2 loading). For each physical quantity, three figures are presented from left to right (e.g., 4a, 4b, and 4c) which correspond to the three exponential factors η = -1, 0, and 1.

While a negative exponential factor corresponds to a stiff surface, a positive factor to a soft surface. It is observed from these figures that, due to different surface loads, the contour magnitudes of the physical quantity are completely different. Interestingly, however, the contour shapes of the vertical elastic displacement u_z and electric potential ϕ are similar in both loading Cases (Fig. 4 vs. 8, Fig. 6 vs. 10). Furthermore, comparing the results for different η, one can also clearly observe that the contour shape changes for different η. For instance, at the same location, the vertical elastic displacement u_z and electric potential ϕ decrease with increasing η (Figs. 4, 6, 8, 10). The field concentration near the edge of the loading on the surface is also demonstrated for the elastic stress and electric displacement components.

7.2 Response of the PFGM multilayered half space to loading Cases 1 and 2

This half space corresponds to the material Model 2 in which the multilayered half space is made of layers with the stacking sequence of PZT-4/PZT-6B/PZT-4. The first PZT-4 layer is functionally graded with exponential factor η = –10, -5, 0, 5 and 10 (Fig. 3). Again, two loading Cases are studied: circular uniform pressure for Case 1 and circular uniform negative charge for Case 2. The vertical elastic displacement u_z, vertical stress σ_{zz},electric potential ϕ, and vertical electric displacement D_z are calculated along the z-axis from the surface (z=0) to the homogeneous half space (z=0.5m), and the results are presented in Figs. 12 to 15, respectively, with (a) and (b) corresponding to the loading Cases 1 and 2.

In the first FGM layer, comparing the responses due to different loading Cases (e.g. Fig. 12a vs. 12b), we noticed that, the trend of variation for the vertical elastic displacement u_z with η is the same. In other words, the vertical elastic displacement increases with decreasing η

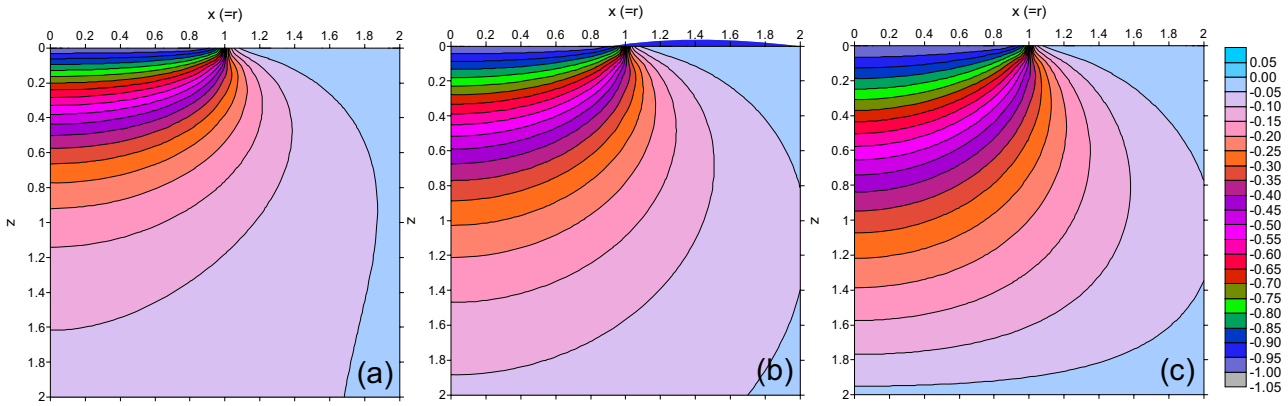

Figure 11 : Contours of the vertical electric displacement D_z in material Model 1 due to the uniform negative charge within the circle of a=1m and magnitude of 1C/m (Case 2). Figures (a), (b), (c) show, respectively, the results for exponential factor η = -1, 0, and 1.

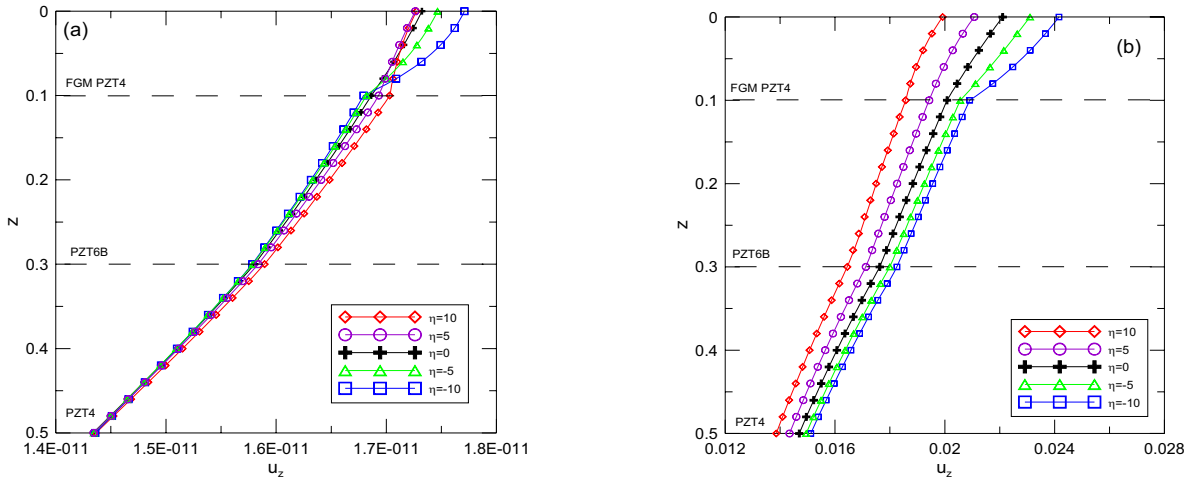

Figure 12 : Variation of the vertical elastic displacement u_z (from (0,0,0) to (0,0,0.5m)) in the PFGM multilayered half space (material Model 2) for the exponential factors η = -10, -5, 0, 5, and 10, respectively. Figures (a) and (b) show the responses due to the uniform surface pressure (loading Case 1) and negative electric charge (loading Case 2), respectively.

for both loading Cases. However, the trend is opposite for the other field quantities under the two different loading Cases. Similarly, in the homogeneous layers (second PZT-6B and PZT-4 half space), the two different loading Cases induce opposite field responses. It is also clear that the response in the underlying homogeneous layers can be greatly affected by the exponential factor η in the first PFGM layer, except for the vertical elastic displacement induced by the pressure loading Case 1 (Fig. 12a) where the influence of the FGM layer is very small in the last PZT half space.

8 Conclusions

In this paper, we derived the solutions of transversely isotropic, piezoelectric functionally graded, and multilayered half spaces due to the uniform circular loading (vertical pressure or negative electric charge) applied on the surface of the half space. The inhomogeneous material is exponentially graded in the vertical direction and can have multiple discrete layers. In the transformed domain, we presented the analytical solution in terms of the propagator matrix method and cylindrical system of vector functions. In order to find the solution in the physical-domain, we introduced and adopted an adaptive Gauss

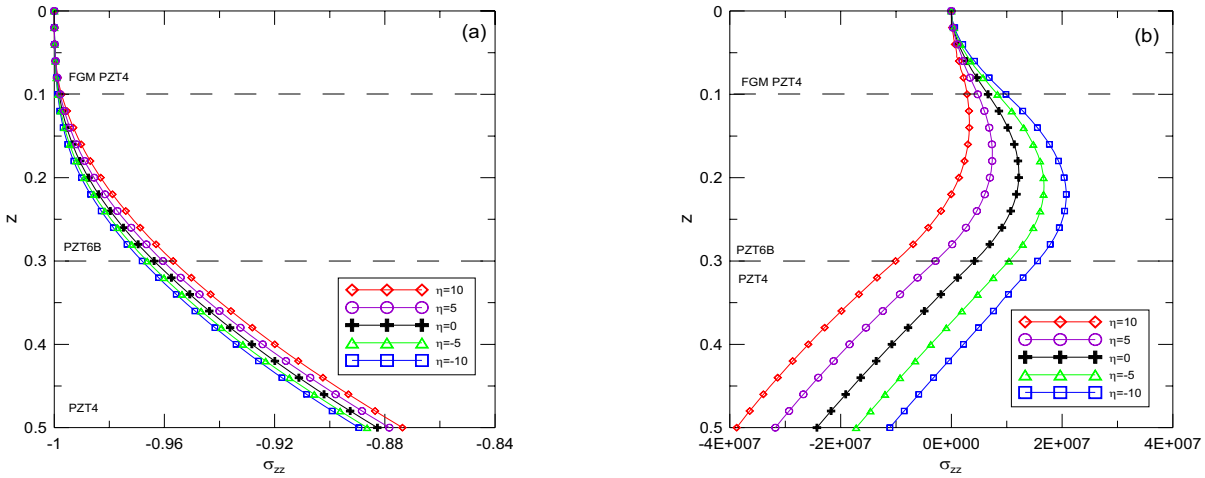

Figure 13 : Variation of the vertical stress σ_{zz} (from (0,0,0) to (0,0,0.5m)) in the PFGM multilayered half space (material Model 2) for the exponential factors η = -10, -5, 0, 5, and 10, respectively. Figures (a) and (b) show the responses due to the uniform surface pressure (loading Case 1) and negative electric charge (loading Case 2), respectively.

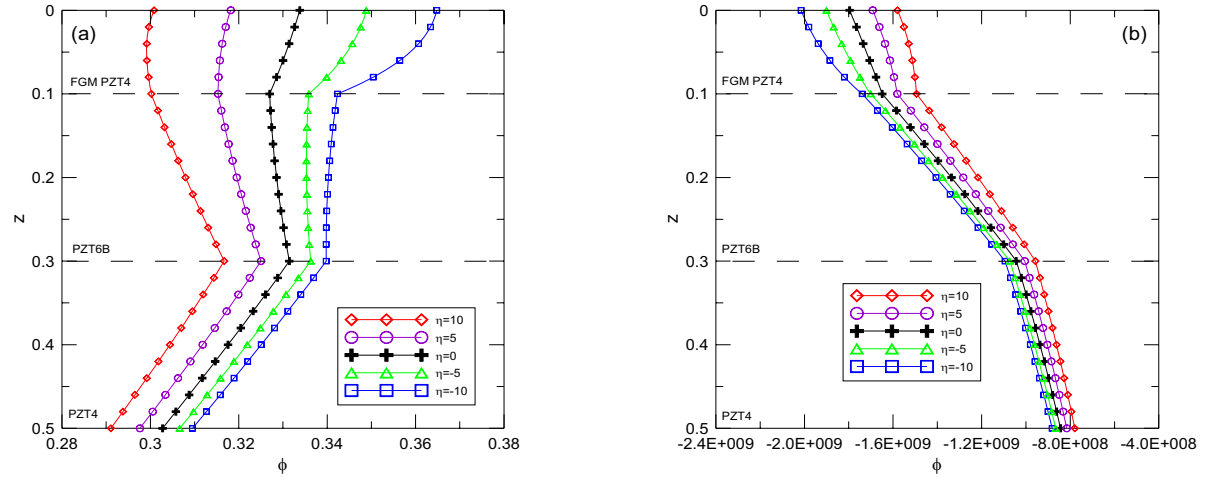

Figure 14 : Variation of the electric potential ϕ (from (0,0,0) to (0,0,0.5m)) in the PFGM multilayered half space (material Model 2) for the exponential factors η = -10, -5, 0, 5, and 10, respectively. Figures (a) and (b) show the responses due to the uniform surface pressure (loading Case 1) and negative electric charge (loading Case 2), respectively.

quadrature with which the one-dimensional infinite integrals of the Bessel function productscan be accurately and efficiently calculated. We finally applied our solutions to two piezoelectric functionally graded half-space models to demonstrate the effect of different exponential factors of the functionally graded material on the field responses. The developed solutions are expected to be useful in the characterization of material properties using indentation tests, and could indirectly contribute to the design and manufacturing of piezoelectric functionally graded structures.

Acknowledgement: The second author (EP) was partially supported by the AFRL Summer Faculty Fellowship in 2005 and by the William Mong Fellowship of HKU in Engineering 2005-2006. The first two authors would also like to thank Dr. Yu at NRL for his kind advice/suggestion during the course of this study and for reading through the first draft of the paper.

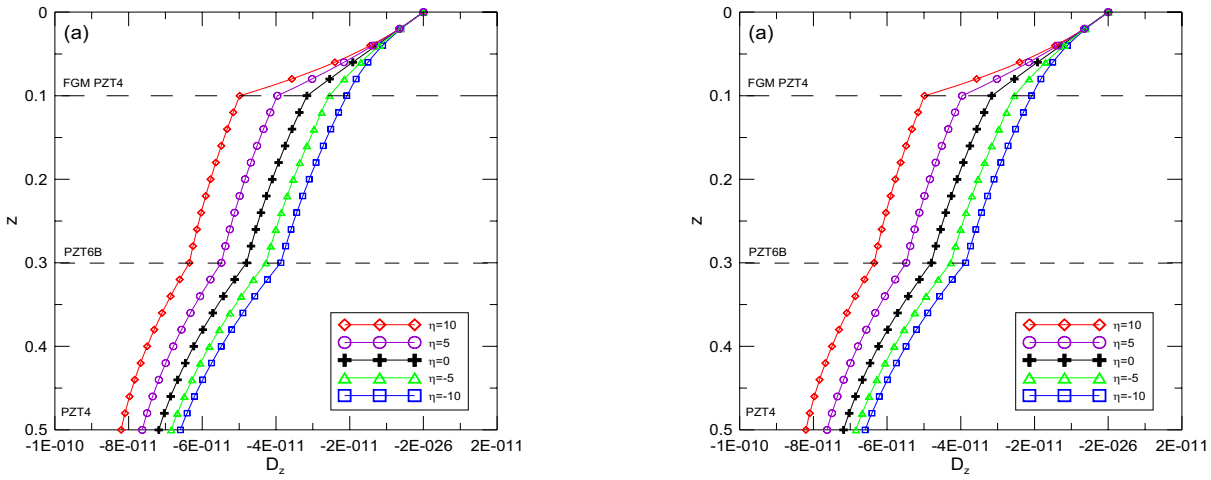

Figure 15 : Variation of the vertical electric displacement D_z along the z-axis (from (0,0,0) to (0,0,0.5m)) in the PFGM multilayered half space (material Model 2) for the exponential factors η = -10, -5, 0, 5, and 10, respectively. Figures (a) and (b) show the responses due to the uniform surface pressure (loading Case 1) and negative electric charge (loading Case 2), respectively.

References

Almajid, A. A.; Taya, M.; Hudnut, S. (2001): Analysis of out-of-plane displacement and stress field in a piezo-composite plate with functionally graded microstructure. *Int. J. Solids Struct.*, vol. 38, pp. 3377–3391.

Almajid, A. A.; Taya, M. (2001): 2D-elasticity of FGM piezo-laminates under cylindrical bending. *J. Intel. Mat. Syst. Struct.*, vol. 12, pp. 341–351.

Atluri, S. N.; Shen, S. (2002); The meshless local Petrov-Galerkin (MLPG) method: A simple & less-costly alternative to the finite element and boundary element method. *CMES: Computer Modeling in Engineering & Sciences*, vol. 3, pp. 11-52.

Balaban, N. Q.; Schwarz, U. S.; Riveline, D.; Goichberg, P.; Tzur, G.; Sabanay, I.; Mahalu, D.; Safran, S.; Bershadsky, A.; Addadi, L.; Geiger, B. (2001): Force and focal adhesion assembly: a close relationship studied using elastic micropatterned substrates. *Nature Cell Biology*, vol. 3, pp. 466–472.

Becker, J. M.; Bevis, M. (2004): Love's problem. *Geophys. J. Int.*, vol. 156, pp. 171–178.

Chan, Y. S.; Gray, L. J.; Kaplan, T.; Paulino, G. H. (2004): Green's functions for a two-dimensional exponentially-graded elastic medium. *Proc. R. Soc. Lond.*, vol. A 460, pp. 1689–1706.

Chave, A. D. (1983): Numerical integration of related Hankel transforms by quadrature and continued fraction expansion. *Geophysics*, vol. 48, pp. 1671–1686.

Chen, Y. H.; Ma, J. (2002): Electrophoretic deposition and characterization of FGM piezoelectric monomorph actuator. In *Proceedings of the Second International Conference on Advanced Materials Processing*, pp. 487–490.

Doherty, J. P.; Deeks, A. J. (2003): Elastic response of circular footings embedded in a non-homogeneous half-space. *Geotechnique*, vol. 53, pp. 703–714.

Gerrard, C. M.; Wardle, L. J. (1973): Solutions for point loads and generalized circular loads applied to a cross-anisotropic half-space. *Technical Paper 13*, CSIRO.

Giannakopoulos, A. E.; Suresh, S. (1999): Theory of indentation of piezoelectric materials. *Acta Mater.*, vol. 47, pp. 2153-2164.

Gilbert, F.; Backus, G. (1966): Propagator matrices in elastic wave and vibration problems. *Geophysics*, vol. 31, pp. 326–332.

Graig, R. F. (1997): *Soil Mechanics*. Taylor & Francis Group, London.

Gray, L. J.; Kaplan, T.; Richardson, J. D.; Paulino, G. H. (2003): Green's functions and boundary integral analysis for exponentially graded materials: Heat conduction. *J. Appl. Mech.*, vol. 70, pp. 543–549.

Hirai, T. (1995): Functional gradient materials, In Materials Science and Technology: A Comprehensive Treat-

ment, *Processing of Ceramics*, Wiley, New York, vol. 17B, pp. 292–341.

Hooper, J. A. (1975): Elastic settlement of a circular raft in adhesive contact with a transversely isotropic medium. *Geotechnique*, vol. 25, pp. 691–711.

Kim, J. H.; Paulino, G. H. (2003): An accurate scheme for mixed-mode fracture analysis of functionally graded materials using the interaction integral and micromechanics models. *Int. J. Numer. Meth. Eng.*, vol. 58, pp. 1457–1497.

Kumar, P. (1988): Nonhomogeneous and cross-anisotropic infinite elements. *Comput. Struct.*, vol. 28, pp. 327–333.

Liew, K. M.; Yang, J.; Kitipronchai, S. (2003): Post-buckling of piezoelectric FGM plates subject to thermo-electro-mechanical loading. *Int. J. Solids Struct.*, vol. 40, pp. 3869–3892.

Lucas, S. K. (1995): Evaluating infinite integrals involving products of Bessel functions of arbitrary order. *J. Comput. Appl. Math.*, vol. 64, pp. 269–282.

Markworth, A. J.; Ramesh, K. S.; Parks Jr, W. P. (1995): Modelling studies applied to functionally graded materials. *J. Mater. Sci.*, vol. 30, pp. 2183–2193.

Martin, P. A.; Richardson, J. D.; Gray, L. J.; Berger, J. R. (2002): On Green's function for a three-dimensional exponentially graded elastic solid. *Proc. R. Soc. Lond.*, vol. A 458, pp. 1931–1947.

Miyamoto, Y.; Kaysser, W. A.; Rabin, B. H.; Kawasaki, A.; Ford, R. G. (1999): *Functionally Graded Materials: Design, Processing and Applications.* Dordrecht: Kluwer Academic Publishers.

Niino, M.; Hirai, T.; Watanabe, R. (1987): The functionally gradient materials. *Japan Society of Composite Materials*, vol. 13, pp. 699.

Oner, M. (1990): Vertical and horizontal deformation of an inhomogeneous elastic half-space. *Int. J. Numer. Analyt. Meth. Geomech.*, vol. 14, pp. 613–629.

Pan, E. (1989a): Static response of a transversely isotropic and layered half-space to general surface loads. *Phys. Earth Planet. Inter.*, vol. 54, pp. 353–363.

Pan, E. (1989b) Static response of a transversely isotropic and layered half-space to general dislocation sources. *Phys. Earth Planet. Inter.*, vol. 58, pp. 103–117.

Pan, E. (1997): Static Green's functions in multilayered half spaces. *Appl. Math. Modelling*, vol. 21, pp. 509–521.

Pan, E.; Yang, B.; Cai, G.; Yuan, F. G. (2001): Stress analysis around holes in composite laminates using boundary element method. *Engineering Analysis with Boundary Elements*, vol. 25, pp. 31–40.

Pan, E. (2002): Mindlin's problem for an anisotropic piezoelectric half space with general boundary conditions. *Proceedings of the Royal Society of London*, vol. A 458, pp. 181-208.

Pan, E.; Han, F. (2004) Green's functions for transversely isotropic piezoelectric multilayered half-spaces. *J. Eng. Math.*, vol. 49, pp. 271–288.

Pan, E.; Han, F. (2005): Green's functions for transversely isotropic piezoelectric functionally graded multilayered half-spaces. *Int. J. Solids Struct.*, vol. 42, pp. 3207–3233.

Pan, E.; Bevis, M.; Han, F.; Zhou, H.; Zhu, R. (2006): Surface deformation due to surface loading of a layered elastic half-space I: A rapid numerical kernel based on a circular loading element, *Geophys. J. Int.* (submitted).

Rodel, J. (2003): Priority Program: Functionally Graded Materials (1995-2002), *Materials Science & Engineering*, vol. A362, Special Issue Nos. 1–2.

Rowe, R. K.; Booker, J. R. (1981): The behavior of footings resting on a non-homogeneous soil mass with a crust, part II circular footings. *Can. Geotech. J.*, vol. 18, pp. 265–279.

Santare, M. H.; Thamburaj, P.; Gazonas, G. A. (2003): The use of graded finite elements in the study of elastic wave propagation in continuously nonhomogeneous materials. *Int. J. Solids Struct.*, vol. 40, pp. 5621–5634.

Selvadurai, A. P. S. (1996): The settlement of a rigid circular foundation resting on a half-space exhibiting a near surface elastic nonhomogeneity. *Int. J. Numer. Analyt. Meth. Geomech.*, vol. 20, pp. 351–364.

Sladek, J.; Sladek, V.; Atluri, S. N. (2000): Local boundary integral equation (LBIE) method for solving problems of elasticity with nonhomogeneous material properties. *Comput. Mech.*, vol. 24, pp. 456-462.

Suresh, S.; Mortensen, A. (1998): *Fundamentals of Functionally Graded Materials*, Institute of Materials, London.

Sutradhar, A.; Paulino, G. H.; Gray, L. J.

(2002): Transient heat conduction in homogeneous and non-homogeneous materials by the Laplace transform Galerkin boundary element method. *Eng. Anal. Bound. Elements*, vol. 26, pp. 119–132.

Wang, C. D.; Tzeng, C. S.; Pan, E.; Liao, J. J. (2003): Displacements and stresses due to a vertical point load in an inhomogeneous transversely isotropic half-space. *Int. J. Rock Mech. Min. Sci.*, vol. 40, pp. 667–685.

Wang, C. D.; Pan, E.; Tzeng, C. S.; Han, F.; Liao, J. J. (2005): Displacements and stresses due to a uniform vertical circular load in an inhomogeneous cross-anisotropic half-space. *Int. J. Geomech.*, vol. 6, pp. 1–10.

Wang, J.; Fang, S.; Chen, L. (2002) The state vector methods for space axisymmetric problems in multilayered piezoelectric media. *Int. J. Solid. Struct.*, vol. 39, pp. 3959–3970.

Xu, J.; Zhu, X.; Meng, Z. (1999): Effect of the interdiffusion reaction on the compatibility of PZT/PNN functionally gradient piezoelectric materials. In *IEEE Transactions on Components and Packaging Technology*, vol. 22, pp. 11–16.

Yu, H. Y. (2001): A concise treatment of indentation problems in transversely isotropic half-spaces. *Int. J. Solids Struct.*, vol. 38, pp. 2213-2232.

Yu, H. Y.; Sanday, S. C.; Rath, B. B. (1990): The effect of substrate on the elastic properties of films determined by the indentation test – axisymmetric Boussinesq problem. *J. Mech. Phys. Solids*, vol. 38, pp. 745-764.

Yue, Z. Q.; Yin, J. H. (1998): Backward transfer-matrix method for elastic analysis of layered solids with imperfect bonding. *J. Elasticity*, vol. 50, pp. 109–128.

Yue, Z. Q.; Yin, J. H.; Zhang, S. Y. (1999): Computation of point load solutions for geo-materials exhibiting elastic non-homogeneity with depth. *Comput. Geotech.*, vol. 25, pp. 75–105.

Appendix A: Appendix A Material properties of PZT-4 and PZT-6B

For the PZT-4, the elastic, piezoelectric, and dielectric coefficient matrices are respectively [Pan, Yang, Cai, and Yuan (2001)]

$$\left[C^0\right] = \begin{bmatrix} 1.39 & 0.778 & 0.743 & 0 & 0 & 0 \\ 0.778 & 1.39 & 0.743 & 0 & 0 & 0 \\ 0.743 & 0.743 & 1.15 & 0 & 0 & 0 \\ 0 & 0 & 0 & 0.256 & 0 & 0 \\ 0 & 0 & 0 & 0 & 0.256 & 0 \\ 0 & 0 & 0 & 0 & 0 & 0.306 \end{bmatrix} \quad (10^{11} N/m^2) \tag{35}$$

$$\left[e^0\right] = \begin{bmatrix} 0 & 0 & 0 & 0 & 12.7 & 0 \\ 0 & 0 & 0 & 12.7 & 0 & 0 \\ -5.2 & -5.2 & 15.1 & 0 & 0 & 0 \end{bmatrix} (C/m^2) \tag{36}$$

$$\left[\varepsilon^0\right] = \begin{bmatrix} 0.64605 & 0 & 0 \\ 0 & 0.64605 & 0 \\ 0 & 0 & 0.561975 \end{bmatrix} (10^{-8} CV^{-1}m^{-1}) \tag{37}$$

and for PZT-6B, they are [Wang, Fang, and Chen (2002)]

$$\left[C^0\right] = \begin{bmatrix} 1.68 & 0.6 & 0.6 & 0 & 0 & 0 \\ 0.77 & 1.68 & 0.6 & 0 & 0 & 0 \\ 0.6 & 0.6 & 1.63 & 0 & 0 & 0 \\ 0 & 0 & 0 & 0.271 & 0 & 0 \\ 0 & 0 & 0 & 0 & 0.271 & 0 \\ 0 & 0 & 0 & 0 & 0 & 0.54 \end{bmatrix} \quad (10^{11} N/m^2) \tag{38}$$

$$\left[e^0\right] = \begin{bmatrix} 0 & 0 & 0 & 0 & 4.6 & 0 \\ 0 & 0 & 0 & 4.6 & 0 & 0 \\ -0.9 & -0.9 & 7.1 & 0 & 0 & 0 \end{bmatrix} (C/m^2) \tag{39}$$

$$\left[\varepsilon^0\right] = \begin{bmatrix} 0.36 & 0 & 0 \\ 0 & 0.36 & 0 \\ 0 & 0 & 0.34 \end{bmatrix} (10^{-8} CV^{-1}m^{-1}) \tag{40}$$